The International Journal of Advanced Manufacturing Technology (2019) 100:877–893
https://doi.org/10.1007/s00170-018-2668-4

ORIGINAL ARTICLE

Investigation on thermal relaxation of residual stresses induced in deep cold rolling of Ti–6Al–4V alloy

Armin Hadadian[1] · Ramin Sedaghati[1]

Received: 4 June 2018 / Accepted: 4 September 2018 / Published online: 29 September 2018

Abstract

In the present study, a finite element model has been developed to simulate the deep-cold rolling process on Ti-6Al-4V specimens and the following short term exposure of the treated components to elevated temperature. The developed model can be effectively used to predict the residual stress profiles induced by the process at room temperature and the following residual stress relaxation at the elevated temperature. In the present study, the thermal relaxation stage is performed using a viscoplastic model which couples the creep and plasticity deformation mechanisms to predict the state of residual stresses at the elevated temperature. For this purpose, a new set of hyperbolic creep law coefficients are identified in order to describe the primary creep at 450 °C. The accuracy of the developed finite element model to predict residual stresses is validated by comparison with the experimental data available in the literature. It has been shown that the finite element predictions correlate well with experimental results with error generally less than 10%. The developed model can be effectively utilized for parametric studies to understand the effect of different process parameters on the induced residual stresses without performing expensive experimental tests.

Keywords Deep cold rolling · Implicit/explicit Lagrangian finite element modeling · Creep and viscoplastic models · Residual stress · Thermal relaxation

1 Introduction

Ti-6Al-4V alloy is a widely used material in highly stressed components at elevated temperatures, such as turbine blades, discs, and aircraft containment structures. Controlling the fatigue failure is of paramount importance and a main challenge in critical components. It is known that the fatigue life of highly stressed component such as turbine blades, crankshafts, and connecting rods can be significantly improved by the introduction of compressive residual stresses and strain hardening in near surface layers [38].

Mechanical surface treatments such as shot peening (SP), liquid jet peening (LJP), laser shock peening (LSP), ultrasonic surface rolling (USRP), low-plasticity burnishing (LPB), and deep-cold rolling (DCR) have been effectively utilized to improve wear resistance, fatigue strength, and corrosion resistance of components by strengthening the material at the surface and introducing a compressive residual stress in the surface layer of the work specimen [2, 4, 26, 39]. DCR in particular is considered to be a low-cost process which is shown to be superior compared with other surface treatment methods, as the profile of the induced residual stresses is generally controllable through the process parameters thus enabling generation of beneficial residual stresses with higher magnitude and depth than the alternative methods. The process also results in a lower surface roughness compared with its counterparts SP and LSP processes [2, 4, 26, 39].

DCR process basically involves the movement of a spherical (or cylindrical) rolling tool on the surface of the workpiece under a controlled, normal force. Figure 1 shows the schematic of the process. The process parameters are rolling speed, rolling feed rate, applied fluid pressure or normal force, and the ball diameter.

The process creates a deep residual stress field beneath the treated surface. A typical residual stress depth profile σ(z) is shown in Fig. 1b which can be characterized by four significant parameters including the residual stress at the surface σ_0

✉ Ramin Sedaghati
ramin.sedaghati@concordia.ca

Armin Hadadian
armin.hadadian@gmail.com

[1] Department of Mechanical, Industrial and Aerospace Engineering, Concordia University, Montreal, Quebec H3G1M8, Canada

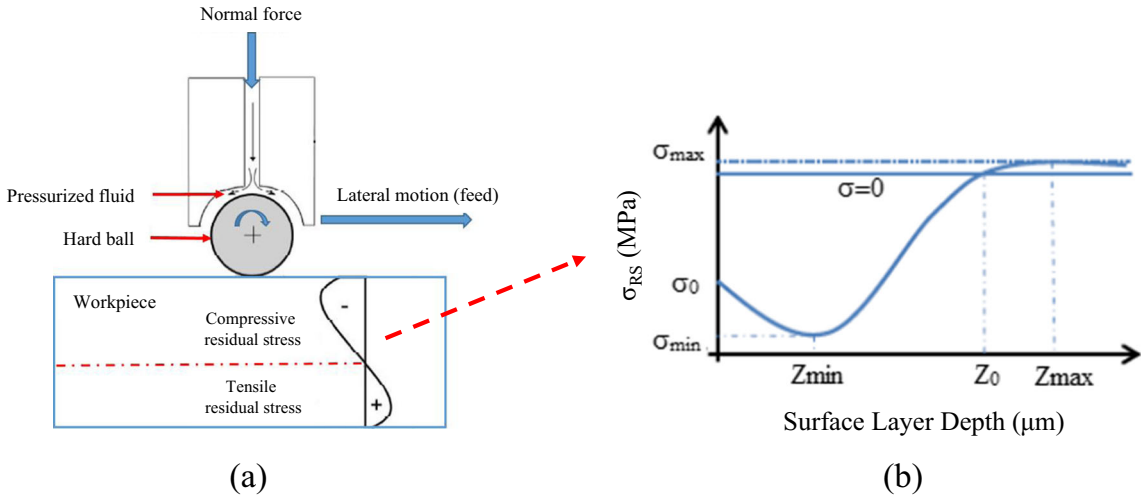

Fig. 1 **a** Schematic of deep rolling process. **b** Characterization of a RS depth profile

(at $Z = 0$), the minimum residual stress σ_{min} located at $Z = Z_{min}$, the maximum residual stress σ_{max} located at $Z = Z_{max}$, and the zero crossing point where the residual stress changes from compressive to tensile ($Z = Z_0$) [38]. It is noted that the residual stress varies through the thickness, and defining stress values on these specified locations will allow better understanding of the nature of the variation and to construct the residual stress profile. Moreover, these parameters can be subsequently used as desired output responses to establish an approximate surrogate response surface model which can be used efficiently for design optimization problems to be investigated in future studies.

It is worth mentioning that deep rolling (DR), deep-cold rolling (DCR), low-plasticity burnishing (LPB), ball burnishing (BB), and roller burnishing (RB) are fundamentally similar surface treatment processes and their differences are either in the tooling design or applied force. Therefore, their naming is interchangeably used in the literature.

The deformation introduced by DCR results in plastic strain, yield surface, and residual stress profiles that vary through the depth from the surface. The process makes three important changes in the near surface layers of a treated material: (1) hardening of the material, i.e., raising the yield strength; (2) large biaxial compressive residual stresses in surface layer constrained by balancing tensile stresses in deeper depth; and (3) severe plastic deformation near the surface layer which may become unstable under cyclic and thermal loads.

The investigation on residual stresses induced by the DCR processing of Ti-6Al-4V alloy has been mainly limited to experimental studies [3, 10, 26, 39] which have unanimously confirmed that the DCR process can effectively improve the fatigue life of components made of Ti-6Al-4V alloy by introducing a deep compressive residual stress and work-hardening near the surface layer of the workpiece even at elevated temperatures [3, 26]. The residual stress induction during the DCR process is the resultant of complex cyclic plastic deformation and microstructural textural evolution occurred on and under layer surface. DCR process is a complex non-linear dynamic phenomenon due to the movement of the ball, the presence of plasticity beneath the rolling ball, and the non-linear contact between the ball and the component. Thus, analysis of the process and the evaluation of the induced residual stresses using analytical methods are not possible. Considering this, numerical techniques based on the finite element (FE) method have been recently utilized to predict the state of residual stress in near surface region developed during the DCR process.

Sayahi et al. [32] simulated the deep rolling process on Ti-6Al-7Nb components using 2D and 3D FE models and compared the simulation and experimental results. The developed 3D FE models provided results with a good agreement with experimental measurements although unable to predict the magnitude of residual stress on the surface. The authors concluded that the 2D FE models only provide a very qualitative description of the RS field and do not yield accurate quantitative results.

Klocke et al. [17] developed a 3D FE model considering a user-defined isotropic hardening model to predict residual stress in Ti-6Al-4V alloy. The developed model underestimates residual stress in the surface layer by more than 50%. Later, Klocke et al. [16] simulated the deep rolling process on Inconel 718 and Ti-6Al-4V specimens assuming non-linear, isotropic/kinematic hardening material models. The FE results showed a good agreement with those of experiments.

Bäcker et al. [4] proposed coupling of the FE method with boundary element (BE) method to perform a time-efficient simulation of deep rolling process on a complete geometry of a turbine blade. It is mentioned that the coupling between FE and BE methods can only be adopted by implicit solvers. Although their methodology can save up to 40% of the time compared to a similar uncoupled FE method, the results of the approach are not quite well matched to the experimental data.

In 2013, Balland et al. [6, 7] concluded that numerical studies on burnishing process had not been successful in describing the effect of the process on surface hardening. They revisited all the assumptions that had been made in prior research work in order to address the drawbacks. Three remarkable conclusions can be outlined based on their results: (1) The residual stress profile evolves gradually by increasing number of rolling passes. (2) A minimum number of rolling passes is required to obtain a stabilized residual stress field. (3) The magnitude of the overlap between the rolling passes has a great effect on the final residual stress state.

Most of the previous research work has been mainly dedicated to the simulation of DCR process performed at ambient temperature. However, majority of highly stressed components treated by this process operate at elevated temperature where beneficial influence of the surface treatments may decrease due to the thermal relaxation of residual stresses at such temperatures.

A non-uniform relaxation of the induced compressive residual stress in thin-walled components can also cause shape distortion and warping in addition to the direct effect of thermal relaxation which is reduction in the amount of compressive residual stress. If the section thickness of the treated component is in the order of the depth of the compressive layer, the distortion could be more severe [29]. This can be a concern in surface treatment of thin turbine blades which any distortion from aerodynamic shape can potentially affect the engine performance and efficiency. Therefore, it is important to investigate and accurately assess the thermal relaxation of the induced residual stresses in such cases.

The thermal relaxation of residual stress is fundamentally due to the annihilation and reorganization of meta-stable crystalline defects induced by treatment process, creep-controlled dislocation rearrangement and material softening at elevated temperatures [42]. Exposure to temperatures above 0.5 *Tm* (melting temperature) for several hours leads to recrystallization of the material. Recrystallization causes grain reformation which relaxes all macro-residual stresses and majority of micro-residual stresses. Stress relaxation at temperatures lower than 0.5 *Tm* is determined by diffusion-controlled dislocation movements and changes from dislocation core diffusion to volume diffusion as temperature raises [33].

The thermal relaxation of the residual stress in deep rolling of Ti-6Al-4V alloy has been experimentally studied [1, 26, 27, 34]. Experimental results show the thermal stability of the residual stresses in the surface layer strongly depends on the material state and particularly on the induced dislocation density. Surface layers with medium dislocation density show enhanced thermal stability of residual stresses while surface layers with extremely high dislocation densities (as induced by shot peening and high ball burnishing pressure) have a poor thermal stability [29, 30].

The microstructure of the subsurface layer in deep-rolled Ti-6Al-4V has a high dislocation density which is thermally unstable [27]. The untreated Ti–6Al–4V has an average α-grain size of about 10 μm and after deep rolling, the nanocrystalline layer with crystallite sizes of about 50 nm is created directly on the surface. The nanocrystalline layer exhibits high dislocation densities and has a complex lamellar substructure [27].

The experimental investigations on deep-rolled Ti-6Al-4V show that the relaxation is greater in the region closer to the surface nearly less than 50 μm from the surface [26, 27], and the relaxation of the stresses on the surface layer is faster than beneath the surface which is fundamentally due to formation of high dislocation densities and nanocrystalline in the surface layer [26, 33].

The initial thermal relaxation is prompt and caused by the change in yield strengths and the Young's Modulus at elevated temperature. Decreasing the Young's Modulus leads to an elastic temporary relaxation. Also with the temperature increase, the yield stress decreases which can be lower than the high compressive residual stresses at room temperature which results in a local plastic deformation causing a permanent residual stress relaxation. It has been shown that the time-dependent thermal relaxation can also be described by creep behavior as shown experimentally for Ti-6Al-4V [14, 34]. Correlation between time-dependent plastic strains and mean residual stress are established in such approach [33].

The DCR process alters the microstructure of the surface layer, and this change will result in a different material behavior. Therefore, plasticity deformation mechanism combined with short-term creep deformation needs to be adopted in the surface layer to model this high rate relaxation mechanism. Similar methodology has been successfully implemented before for FE modeling of thermal relaxation of shot-peened Nickel-base supper alloy [8].

A comprehensive literature review conducted for the current research work revealed that the available published numerical studies are mainly limited to simulation of the process to predict the induced residual stresses at the ambient temperature. Moreover, the accuracy of the previous numerical results especially in the region closer to surface layer is not sufficient when compared with available experimental data. And most importantly, they have not addressed further relaxation of the induced residual stresses under specific thermomechanical environments.

Despite experimental studies, to the best of our knowledge, there is no prior published work detailing the modeling of the thermal relaxation of residual stresses in deep cold rolled Ti–6Al–4V alloy with a systematic validation with the experimental results.

The objective of the current study is to develop a reliable FE model and simulation codes for predicting residual stresses associated with the DCR process and the following thermal relaxation at elevated temperature of 450 °C.

2 Simulation framework

As mentioned before, due to highly nonlinear cyclic plastic deformation and contact between the ball and the component, simulation of DCR process to evaluate the induced residual stress field cannot be determined by means of analytical methods and thus the use of high-fidelity FE-based models is inevitable. In the present work, a high-fidelity 3D FE model has been developed in ABAQUS software to not only simulate the DCR process in order to predict the residual stress but also to determine thermal relaxation of these induced residual stresses at elevated temperatures.

ABAQUS package generally offers two powerful solvers namely ABAQUS/Standard and ABAQUS/Explicit. ABAQUS/Standard uses the iterative procedure based on the implicit time integration technique which is unconditionally stable but is slow convergent especially for short duration dynamic non linear problems. On the other hand, ABAQUS/Explicit is based on explicit time integration technique, which is conditionally stable. However, with properly selected time step, the explicit solver can be effectively used to solve complex non linear dynamic problems with fast convergence [37].

The proposed simulation framework has been divided into three main stages as shown in Fig. 2. First, the DCR process at room temperature is simulated assuming Johnson Cook material model to evaluate the induced residual stress and strain fields which are then subsequently considered as initial conditions for the next stage of simulation in which the spring-back analysis is modeled using isotropic plasticity behavior of the material at a low strain rate. The results of this stage are validated to those available experimental measurements.

The output of spring-back analysis is the initial states for the thermal relaxation assessment where the effect of the elevated temperature on the induced residual stress field is modeled through the plastic softening and short-term creep relaxation mechanism. The results obtained from the analysis of this step are also compared to those available experimental measurements for the purpose of validation of the developed FE model. This stage includes several sequentially coupled steps in which the stress and strain output of each step will be an initial state for the following step.

As explained earlier, modeling of DCR inherits many sources of non-linearities mainly due to the contact analysis, non-linear behavior of the material, dynamic loading, and large deformation. ABAQUS is capable of handling highly dynamic non-linear problems efficiently and accurately using its explicit module and has shown to be effective in modeling DCR process [25, 43]. It is noted that spring-back and thermal relaxation stages, due to their quasi-static nature, are analyzed in ABAQUS/Standard.

3 Solution of governing equations using explicit and implicit methods

The final governing equations in the finite element format at a specific instant of time may be described as

$$M\ddot{u} + I - P = 0 \tag{1}$$

where M is mass matrix, and I and P are internal and external force vectors, respectively. $\ddot{u}$ represents the nodal acceleration vector. Direct integration methods are used in ABAQUS to solve time history analysis and are generally categorized into explicit and implicit methods.

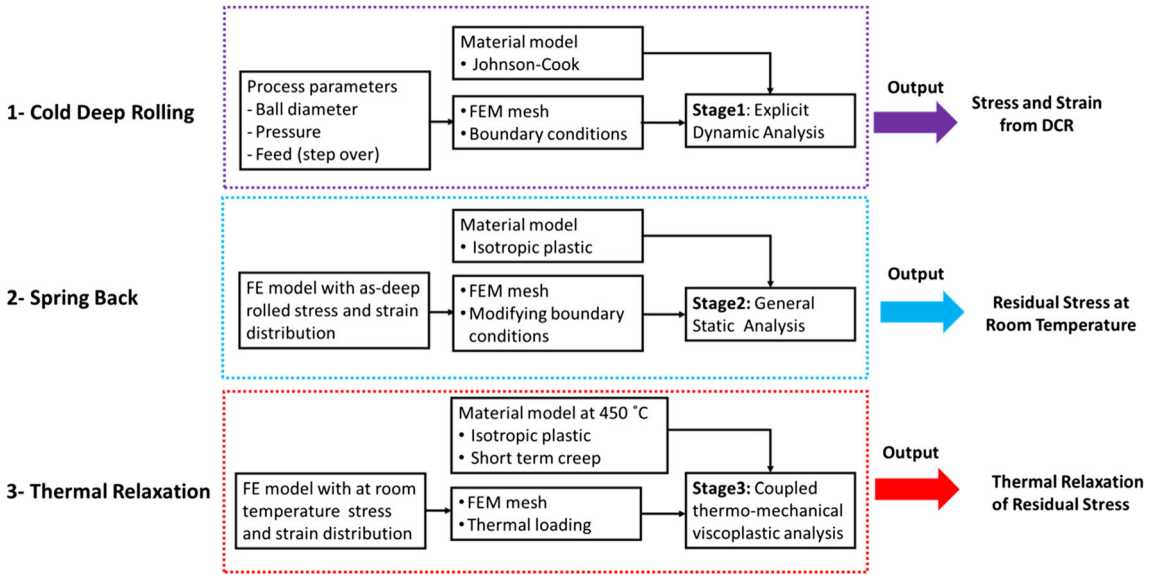

Fig. 2 Flow chart for the simulation of the DCR process and thermal relaxation

3.1 Explicit method

The central difference time integration algorithm is mainly used in ABQUS/Explicit [37] to integrate through time by using many small-time increments.

ABAQUS/Explicit solves state of dynamic equilibrium at the beginning of the current time increment, described by

$$M\ddot{u}^{(i)} + I^{(i)} - P^{(i)} = 0 \tag{2}$$

where the superscript (i) refers to the increment number. Explicit analysis employs first-order elements with "lumped" mass matrix property (diagonal mass matrix) which enhances computational efficiency. Therefore, the calculation of the nodal accelerations can be straightforward by using the inverse of the mass matrix as

$$\ddot{u}^{(i)} = M^{-1}.\left(F^{(i)} - I^{(i)}\right) \tag{3}$$

The explicit central difference integration method is then employed to update the velocities and displacements per following steps:

$$\text{Step 1}: \quad \dot{u}^{\left(-\frac{1}{2}\right)} = \dot{u}^{(0)} - \frac{\Delta t^{(0)}}{2}\,\ddot{u}^{(0)} \tag{4}$$

$$\text{Step 2}: \quad \dot{u}^{\left(i+\frac{1}{2}\right)} = \dot{u}^{\left(i-\frac{1}{2}\right)} + \frac{\Delta t^{(i+1)} + \Delta t^{(i)}}{2}\,\ddot{u}^{(i)} \tag{5}$$

$$\text{Step3}: \quad u^{(i+1)} = u^{(i)} + \Delta t^{(i+1)}\,\dot{u}^{\left(i+\frac{1}{2}\right)} \tag{6}$$

where $u, \dot{u}$ and $\ddot{u}$ are the vectors of nodal displacement, velocity, and acceleration, respectively. The equations of motion are integrated using a central difference integration rule. Thus, using Eq. (6), the displacement vector at any time increment can be calculated explicitly from the previous displacement, velocity and acceleration vectors. The time increment must be smaller than the time required for a dilatational wave to cross any element in the mesh which is estimated as

$$\Delta t \leq \frac{L_{\min}}{\sqrt{E/\rho}} \tag{7}$$

in which L_{min} is the smallest element dimension in the FE model and ρ and E are the density and Young modulus of the material, respectively. Therefore, the size of the smallest element in the FE model dominates the stable time increments. Although the time increments are typically very small compared to the cycle time of forming processes, the computation time for each time increment in the explicit procedure is very short because the solution requires no iterations.

The explicit method could be computationally very expensive for quasi-static problems such as metal-forming processes because it requires a long-time solution and needs very small elements in the contact zone due to a high level of non-linearity. The run time of dynamic explicit program can be further reduced by artificially increasing the forming rate (time scaling) or artificially increasing the density of the elements (mass scaling technique). However, the solution accuracy can be compromised because of the introduction of unrealistic dynamic effects if proper care is not taken using these techniques. The kinetic energy of the system needs to be carefully monitored through the simulation process to ensure that the ratio of kinetic energy to internal energy does not exceed 10%. Time-scaling approach should not be used in a strain rate-dependent simulation like deep rolling process [37].

It is noted that the stable time increment depends on the material properties as shown by Eq. (7) and the element size. The time increments are governed by the elements in the layer close to the surface through the analysis process because they have the smallest size and their size changes due to loading. It is noted that the mass scaling technique with the target time increment of 8×10^{-8} has been employed in the current work.

3.2 Implicit method

The implicit numerical procedures are usually unconditionally stable and the Newmark family of methods is the most popular and widely used implicit methods [9]. Implicit solver available in ABAQUS/Standard for time integration of the dynamic problem uses the backward Euler operator and a generalized form of Newmark method. The method implements a controllable numerical damping to provide automatic dissipation of high-frequency numerical noise which allows the numerical stability and automation of time stepping scheme [37]. The Newmark methods calculate the nodal displacement and velocity as follows [9]:

$$(u)^{i+1} = (u)^{i} + \Delta t(\dot{u})^{i} + \Delta t^{2}\left(\left(\frac{1}{2} - \beta\right)(\ddot{u})^{i} + \beta(\ddot{u})^{i+1}\right) \tag{8}$$

$$(\dot{u})^{i+1} = (\dot{u})^{i} + \Delta t\left((1-\gamma)(\ddot{u})^{i} + \gamma(\ddot{u})^{i+1}\right) \tag{9}$$

with

$$\beta = \frac{1}{4}(1-\alpha)^{2}, \gamma = \frac{1}{2} - \alpha \quad \text{and} - \frac{1}{2} \leq \alpha \leq 0. \tag{10}$$

A large system of equations is solved repeatedly at each time step to obtain the displacement field. As it can be realized from Eq. (8), the displacement field at step $i+1$ depends also on the acceleration on step $i+1$ demonstrating the implicit nature of the method.

As mentioned before, the DCR process is a highly non-linear dynamic phenomenon in which the non-linearity is mainly due to the geometric and material non-linearity as well as contact between the rolling ball and the workpiece. The non-linearity translates itself into variable stiffness matrix which depends on current nodal displacement vector. Thus,

at each time step, in non-linear dynamic problems, an iterative procedure requires to obtain the nodal displacement vector which is generally accomplished using the Newton Raphson method. This issue in addition to the iterative nature of time steps for dynamic analysis makes simulation of DCR process highly computationally expensive for the implicit solvers.

Although there is no restriction on time step size in the implicit method, it should be generally kept small to fulfill equilibrium after each incremental step. In a complex problem with rapidly changing contact conditions like DCR, implicit codes are computationally very expensive because of huge number of iterations required to satisfy the equilibrium at each time increment. In contrast to the implicit solver that each increment typically requires several iterations to obtain a solution within a defined tolerance error, employing small time increments in explicit solver allows the solution to proceed without iteration and forming tangent stiffness matrices in each time increment which significantly simplifies the treatment of contact problems.

Considering above in the present study, the DCR process is modeled using explicit solver available in ABAQUS /Explicit package. After removing the rolling element (spring back stage), the non-linearity due to the contact between the tool and the workpiece does not exist anymore and the workpiece approaches the steady-state condition slowly. Thus, the implicit solver available in ABAQUS/Standard package can be effectively employed to analyze the spring-back stage of the simulation in which the state of stress in the last step calculated in the ABAQUS/Explicit is imported into ABAQUS/Standard [37].

4 Finite element simulation of DCR at room temperature

As mentioned before in the introduction section, the rolling process should be simulated by a 3D FE model since nature of the rolling contact is three-dimensional and no symmetry can be found in order to reduce it to 2D problem [13]. The influence of deep rolling on the workpiece is highly localized so the effect of surface curvature and the resultant helical rolling path is negligible in the modeling of DCR process on a cylindrical workpiece [31, 40]; therefore, the process can effectively be modeled on a flat plate without sacrificing the accuracy.

The pressurized fluid acts as the coolant and lubricant in the process. Thus, the process is assumed to be isothermal [31] and for the interaction between the workpiece and ball, a frictional coefficient between 10^{-5} and 5×10^{-3} is considered using isotropic Coulomb friction model [20].

In the present study, a high-fidelity 3D FE model has been developed to simulated DCR process to evaluate the induced residual stresses at room temperature and subsequently to investigate the relaxation of the residual stresses at the elevated temperature. Figure 3 shows the 3D FE model of the ball and the workpiece developed using C3D8RT elements in ABAQUS environment. C3D8RT is an 8-node thermally coupled brick element accommodating temperature degree of freedom (DOF) in addition to all possible displacement DOFs. Stresses are evaluated at the Gauss points with reduced integration to prevent shear locking. The DCR process parameters are considered to be the ball diameter, rolling force, and feed. The process parameters of experimental work of Nalla et al. [26] were considered for the modeling in order to validate the FE results.

The experimental results show that the DCR process can induce the residual stresses with high gradient up to 600 μm depth from the surface of the workpiece. Hence, a very refined mesh (size of 25 μm) has been used in the vicinity of contact zone as shown in Fig. 3 to achieve accurate results. However, in the regions far away from the contact zone, coarser elements were used to decrease the number of degrees of freedom and computational costs.

The geometry of the workpiece was partitioned to smooth the transition from very refined mesh to coarse mesh in order to avoid element distortion and generate a high-quality mesh. As the hardness of the moving ball is generally several times higher than that of test specimen, it has been modeled as analytical rigid body and hence its motion can be associated to a reference point. This assumption reduces the number of degrees of freedom required to describe the motion of the rolling ball making the simulation more computationally efficient without compromising accuracy.

A series of simulation cycles are conducted until a stable residual stress field is achieved in the contact zone. The roller kinematics is defined by four different boundary conditions as

1. Indentation step where the ball is pushed in to the surface of workpiece

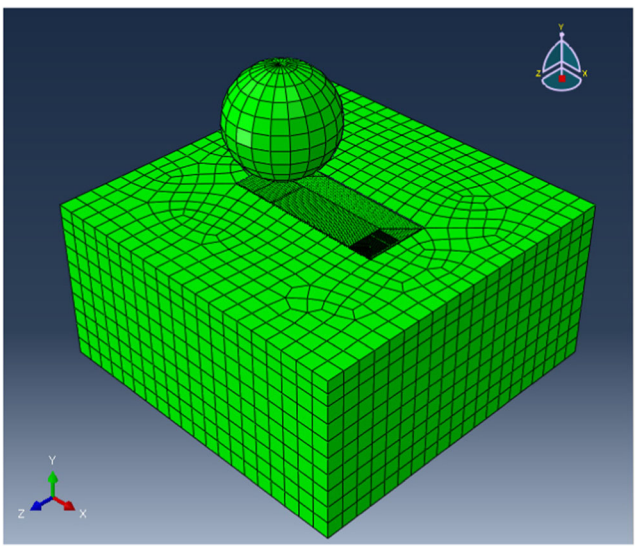

Fig. 3 Geometric model and mesh of the workpiece in the 3D simulation

2. Rolling steps whereby the ball is free to rotate while the force is constantly applied
3. Overlap steps where the ball is offset laterally (perpendicular to the rolling pass) by the amount of feed. In this step, the movement of the ball in the other directions is fixed
4. Retraction step where the ball is removed from the surface

When the ball rolls and finishes one trajectory in X direction, it is then offset in Z direction and rolls back in an opposite direction (−X) to complete the next trajectory. Through several trial and errors, 10 numbers of rolling passes was found sufficient to reach a stable stress state.

The accuracy of the predicted residual stresses significantly depends on the reliability of the constitutive model used to describe the material cyclic inelastic behavior [43]. The calculated rolling contact stress and the components of the residual stress and strain are significantly influenced by the assumed plasticity model for the workpiece. For the simulation of multi-pass surface rolling process, the material model should be able to demonstrate work-hardening effect as a result of plastic deformation, strain rate hardening effect caused by rate of the loading, and the cyclic deformation behavior at ambient temperature [22]. Available material models which can be effectively used in deep rolling processes include Lemaitre-Chaboche-Plasticity (LCP) model and Johnson-Cook (JC) model.

The JC model is purely empirical and its ability to adequately represent the deformation and failure of Ti-6Al-4V during high-rate loading, as well as large changes in strain rate and temperature has been approved [19]. The model can be described as

$$\sigma = [A + B\varepsilon^{n}]\left[1 + C\ln\dot{\varepsilon}^{*}\right]\left[1-\left(\frac{T-298}{T_m-298}\right)^{m}\right] \tag{11}$$

where σ and ε are the effective stress and strain respectively; $\dot{\varepsilon}^{*}$ is the normalized effective plastic strain rate; n is the work-hardening exponent; and A, B, C, and m are constants which are determined from an empirical fit of flow stress data . T_{melt} represents the melting temperature.

It should be noted that JC model parameters are evaluated using a number of experimental tests at different strain rates and temperature. JC model provided in Eq. (11) has three distinct parts (inside brackets) which explicitly relates the stress to strain, strain rate, and temperature, respectively. The parameters A, B, and n can typically be evaluated using quasi-static tests or dynamic tests at very low strain rate. Once these parameters are identified, then parameters C and m which relate the strain-rate and temperature-dependent part of JC model to temperature, respectively, should be identified using series of dynamic tests at various controlled strain rates and temperatures from low to very high. This can be conducted using apparatus such as Split-Hopkinson Bars or Tayler Impact Test.

The JC model has been extensively used to describe the material behavior in the simulation of cold rolling processes [28] and has been particularly studied to describe the Ti-6Al-4V strain-hardening behavior under various temperature and strain rates [15, 36]. Therefore, the JC constitutive material model has been considered to model the stress-strain behavior of Ti-6Al-4V alloy in this study. Numerous sets of JC model parameters exist for Ti-6Al-4V in the literature [15, 36] where each set has been defined based on the measured plastic strain and strain rates in a specific range of temperatures. The assumed JC model for the simulation of the DCR process should cover the largest strain and strain rate typically generated during the process. Thus, the JC model developed by Lee and Lin [18] for Ti-6Al-4V with parameters presented in Table 1 was adopted in this study.

When the deep rolling process is completed, the stress and strain fields calculated at the end of the ball retraction are then transferred to an implicit FE model to determine the settled residual stress in the component. This stage of the process, which is called spring back, is quasi-static in nature, and therefore plastic material model at lower strain rate is required in the simulation. Thus, the true stress and strain curves at strain rate 1 s^{-1} at room temperature, reported by et al. [11], has been implemented in form of isotropic plasticity in the FE model to carry out the spring-back analysis. This isotropic plastic model was also used in the DCR simulation later to investigate the effects of the assumed plasticity model on the predicted residual stress profile.

5 Validation of the FE model

In this study, the experimental results reported by Nalla et al. [3, 26] are used to validate the developed FE models. They performed deep rolling on Ti-6Al-4V rod with the diameter of 7 mm using a 6.6-mm diameter ball under rolling pressure of 150 bar (15 MPa) and constant feed of 0.1125 mm per revolution followed by annealing at 450 °C for 45 min. The X-ray diffraction (XRD) method was then used to measure the residual stress induced by DCR process and to measure the residual stress after the following thermal relaxation.

Lattice spacing variation is measured using Bragg law and compared to a strain-free reference specimen to calculate residual stress and strains in XRD technique. This method involves material layer removal which causes inevitable relaxation and redistribution of the initial residual stress profile. Stresses in both directions tend to fall to zero after layer removal since all the volume where residual stresses balanced

Table 1 JC material constant parameters presented for Ti-6Al-4V [18]

A (MPa)	B (MPa)	n	C	m
724.7	683.1	0.47	0.035	1

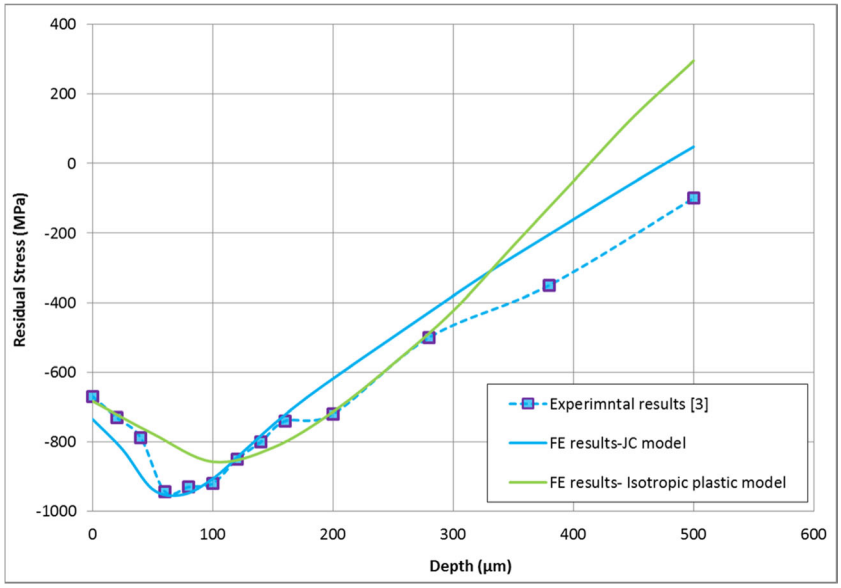

Fig. 4 Comparing tangential residual stress profile through the depth obtained using FE and experiment at room temperature

themselves are removed. Therefore, the measurement error increases with the depth from the surface. Additionally, measuring tensile residual stresses beneath the surface using XRD method is not possible due to this layer removal approach. The equilibrium of forces between the tensile region and compressive region must be maintained in each step and due to layer removal, the compressive region either reduces or does not exist [35]. Also, residual stress measurement techniques are more or less inefficient in measuring the residual stress in curved directions [24].

The residual stress in the rolling direction (axial) is considerably lower than that in perpendicular to the rolling direction (tangential). Therefore, only the residual stresses measured in tangential directions have been reported [26, 39] and will be used here to validate the FE model.

Figure 4 shows the comparison of the tangential residual stress profile predicted by the developed FE model and the experimental measurements of Nalla et al. [3, 26]. Both JC and isotropic plastic models have been used as the material constitutive models in the developed FE model. As it can be observed, predicted residual stress profile based on the JC model agrees very well with that obtained experimentally up to depth of 170 µm. Specifically, the magnitude of the residual stress at the surface and also the maximum induced residual stress and its location beneath the surface have been accurately predicted. While FE model based on the isotropic plastic

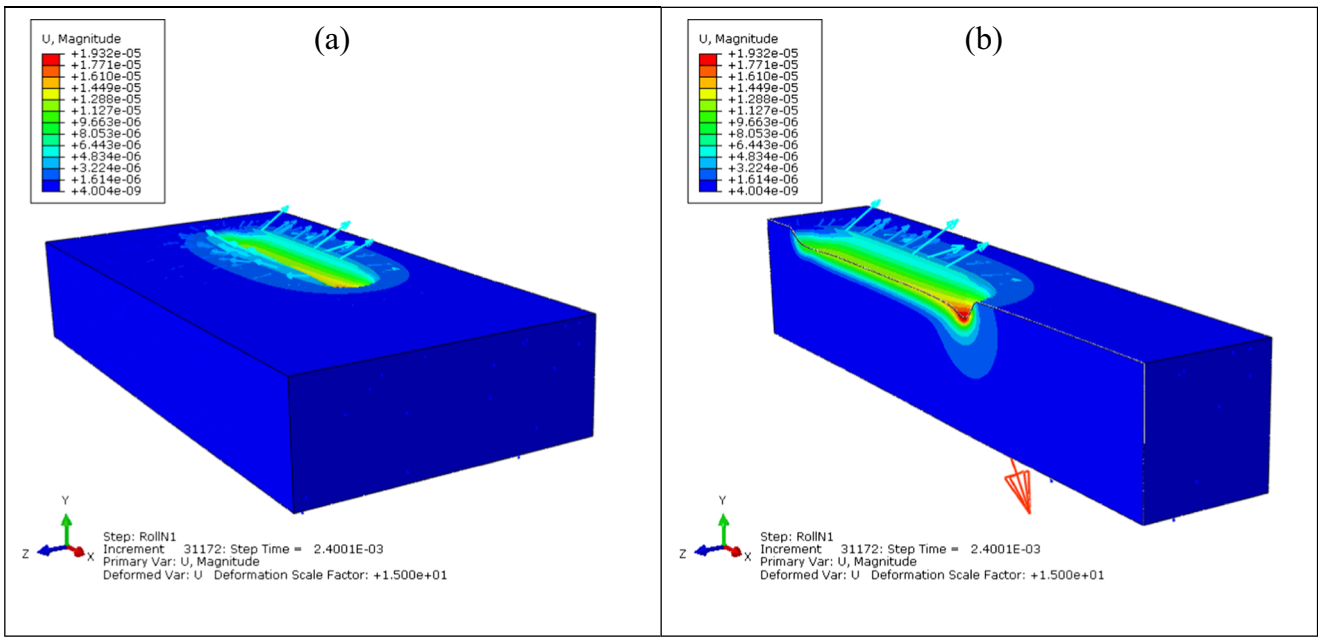

Fig. 5 Displacement magnitude (*m*) with material flow vectors (**a**) and its sectioned view (**b**)

model was able to accurately predict the residual stress on the surface, it was not capable of capturing the location and magnitude of the maximum residual stress.

The difference between the simulation results for the residual stress and those reported experimentally at the deeper locations (beyond 170 μm) below the surface may be attributed to the fact that the residual stresses measured in the experiments have not been corrected to account for layer removals [26]. The residual stresses are self-equilibrating in surface-treated components. As a result, by removing each layer of compressive residual stress in XRD processes, the magnitude of the remaining compressive stresses must increase to satisfy the equilibrium with the intact tensile stress in deeper depth of the component. Therefore, when the amount of measured compressive stresses is not corrected for the effect of the layer removal, the depth of the compressive layer and the measured compressive residual at each depth may be greater than the real value.

5.1 Effect of the rolling pass on the residual stress distribution

Here, the effect of rolling ball movement on the induced residual stress is investigated. The process parameters are ball diameter of 6.6 mm, pressure of 150 bar (15 MPa), feed of 0.1125 mm, and rolling speed of 700 mm/s which were taken from the experimental study published by Nalla et al. [3, 26]. Figure 5 shows the displacement magnitude contours and material flow vectors after the first rolling pass. When the ball rolls, the flow of material in the z direction is restrained by the surrounding material which forms lateral protrusions on each side of the created groove. As illustrated in the figure, the

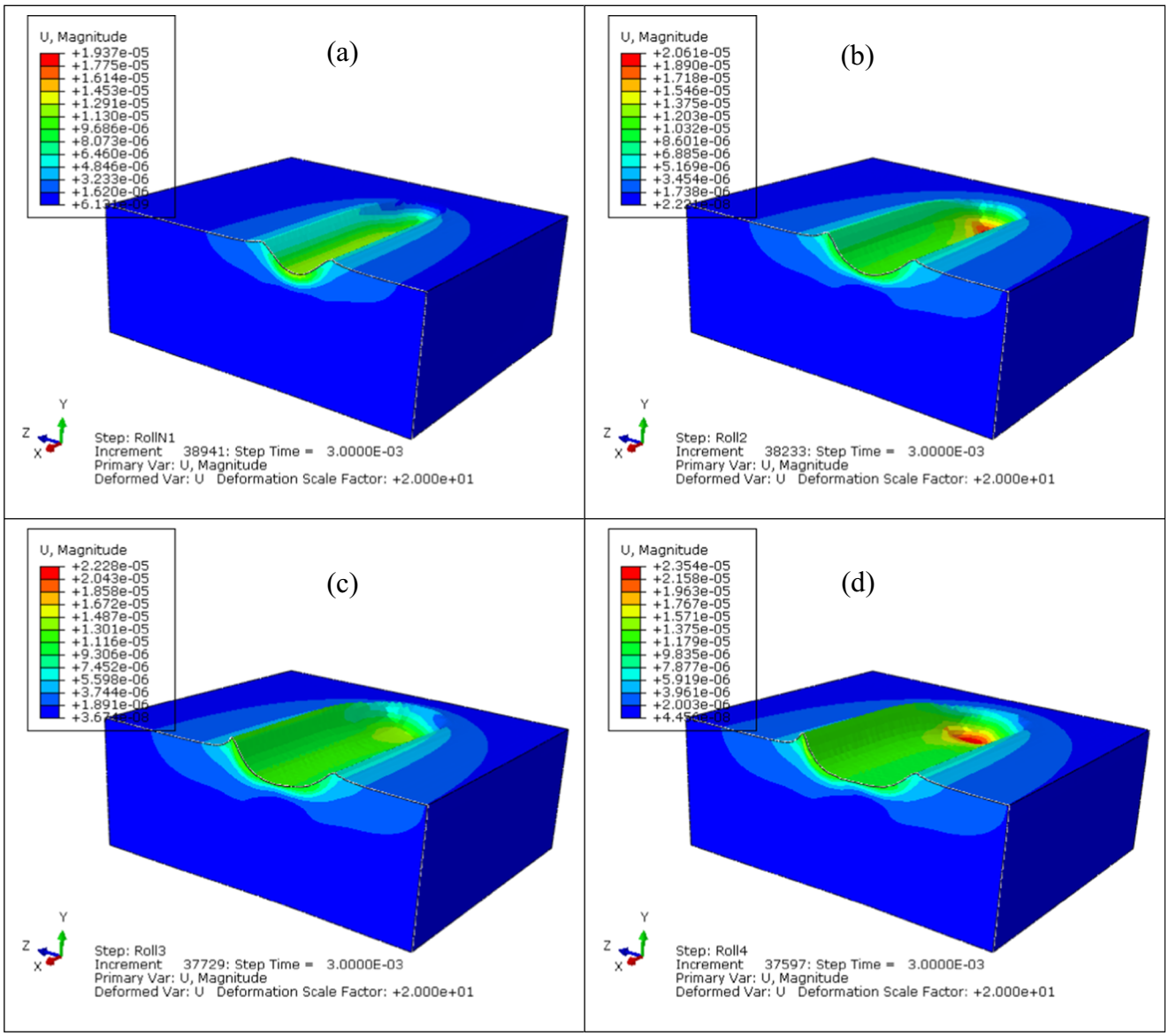

Fig. 6 Resultant displacement (m) contour after one (**a**), two (**b**), three (**c**), and four (**d**) rolling pass

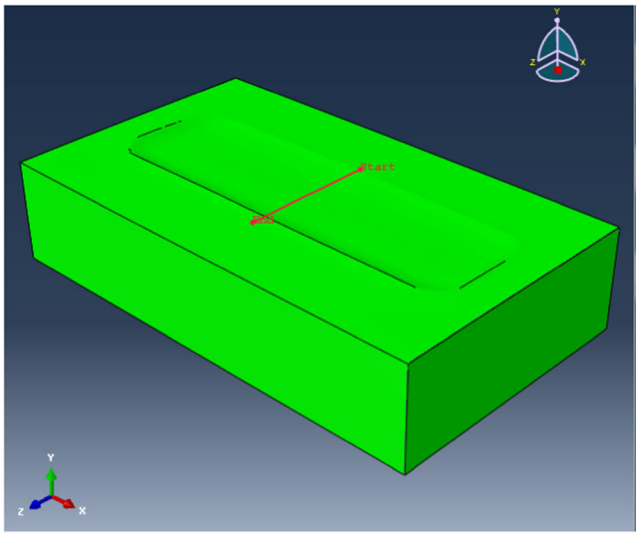

Fig. 7 Mid-span line on which the displacement in *y* direction has been evaluated during each rolling pass

heights of the protrusions on the sides of the groove are greater than the height of the front ridge which explained why the residual stress in tangential (z) direction is greater than the rolling (x) direction.

The lateral protrusions rising in the first rolling pass will interact with the ball movement during the next trajectory. In another word, the ball in the subsequent pass has to move over a surface deformed by the previous rolling pass which also inherits plastic hardening. Therefore, the generation of the lateral protrusions in the following trajectory is influenced by the already existing protrusions due to strain hardening and generated roughness in previous passes. The succeeding rolling also lifts up the bottom of the groove created by the previous passage. This can be easily observed from Fig. 6 which shows the evolution of the surface profile in the first four rolling passes at the end of each cycle. It is noted that the deformed shapes are scaled by 20 for the sake of clarity.

In order to investigate the saturation stage whereby increasing the number of rolling passes the surface profile becomes stable, the displacement in mid-span of the rolling trajectory was extracted in y direction (normal to the surface) in the yz plane. Figure 7 shows the line where the displacement in y direction has been investigated. The y-displacements of the nodes located on the entire mid-span line as shown in Fig. 7 are evaluated after each rolling pass, and the results are shown in Fig. 8. As it can be realized, the displacements in the range between $z = 500$ and 1000 μm are nearly constant.

Examination of Fig. 8 reveals that the displacement profile has evolutionary characteristics and strongly depends on the number of rolling passes. After several simulations, it has been observed that the displacements and subsequently induced residual stresses stabilize after eight rolling passes.

5.2 Residual stress profiles

Figure 9 shows the residual stress in tangential direction (σ_{zz}) after spring-back sectioned in the stabilized region, corresponding to $z = 400$–700 μm in Fig. 8. Nine vertical lines (normal to the surface) are used to obtain the residual stress distribution through the thickness, and the calculated average values are compared to experimental results as presented in Fig. 4. It should be noted that due to very high numerical computation time, we have selected only 10 as the number of passes which covers a part of the surface but it is enough to develop a stabilized region to extract the results.

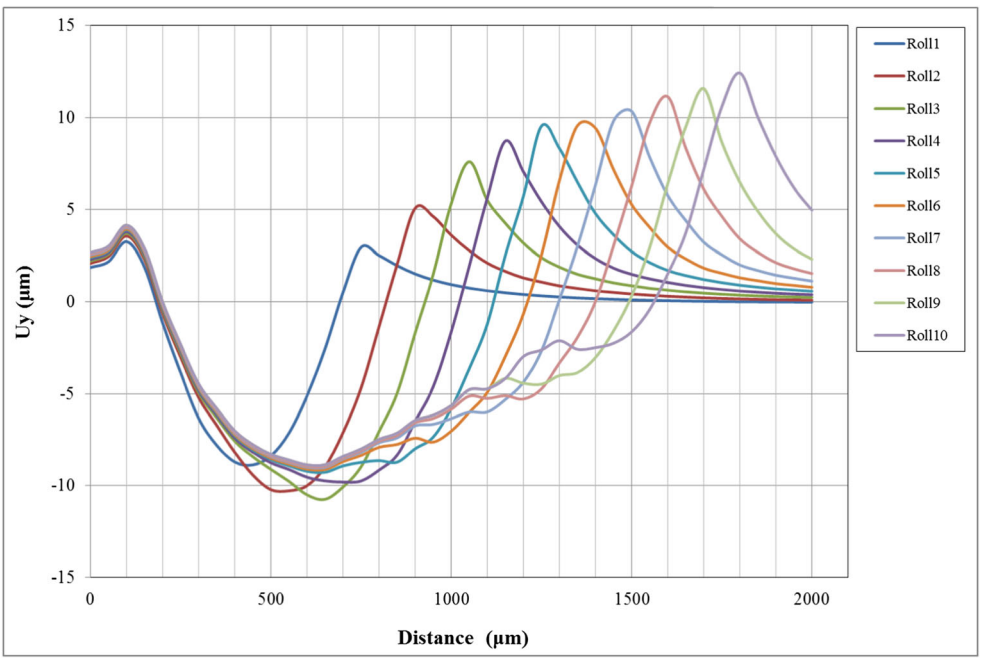

Fig. 8 The evolution of surface profiles in *yz* plane (perpendicular to the work piece surface) at the mid-span during each cycle of rolling

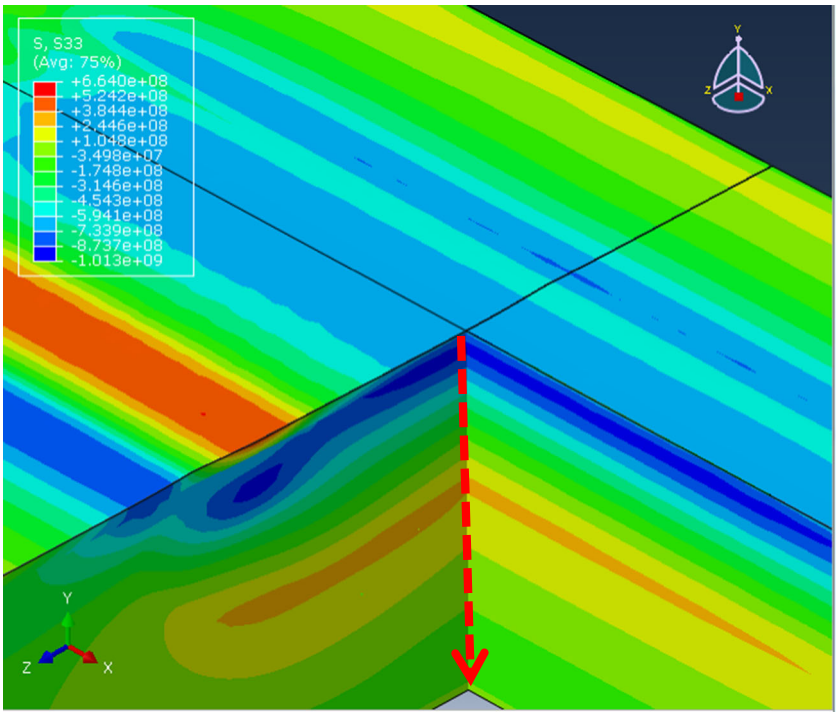

Fig. 9 Residual stress (Pa) in tangential direction (σ_{zz}) after spring-back sectioned in the stabilized region

The residual stress distribution in the axial (σ_{xx}) and tangential (σ_{zz}) directions in the stabilized region (seen in blue color in Fig. 9) are shown in Fig. 10. As it can be seen, DCR process develops very different residual stress distribution through the depth along longitudinal and transverse directions.

The predicted residual stresses in axial and tangential directions illustrated in Fig. 10 have been quantified using parameters defined in Fig. 1b and are highlighted in the plot and presented in Table 2. According to the presented results, the magnitude of the tangential residual stress is almost three times of the axial residual stress at the surface and the magnitude of $(\sigma_{min})_{zz}$ is approximately 35% higher than the magnitude of $(\sigma_{min})_{xx}$. This is in a very good agreement with experimental observations published by Liam et al. [21] where approximately 2.8 and 35% had been respectively reported. The comparison of Z_{min} and Z_0 values presented for tangential and axial directions shows that the axial residual stress is developed in a deeper depth compared with that of tangential residual stress.

It has also been observed that the amount of feed, which controls the overlap between the two following rolling passes,

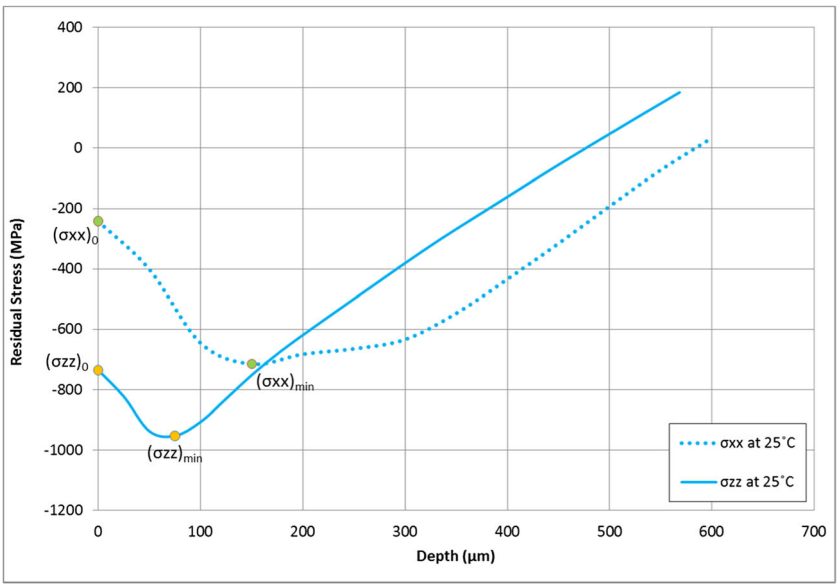

Fig. 10 Residual stress profiles in axial and tangential direction at room temperature

Table 2 Characterization of residual stress depth profiles plotted in Fig. 10

	Tangential (Z direction)	Axial (X direction)
σ_0 (MPa)	723	214
σ_{min} (MPa)	943	714
Z_{min} (μm)	75	150
Z_0 (μm)	480	580

has a significant effect on the final state of the residual stress. To demonstrate this, the effect of feed on the residual stress profile has been investigated while the other process parameters were kept unchanged. The effect of the feed on tangential residual stresses σ_0 and σ_{min} is shown in Figs. 11 and 12, respectively. Results show a parabolic relation between the introduced residual stresses and the feed.

Statistical analysis of the effect of feed on work hardening surface hardness in ball burnishing process shows that the surface hardness increases linearly by increasing the feed [23]. Prevéy has shown that a parabola function best fits the relation of measured residual stresses with respect to hardness measurements by the full width at half maximum (FWHM) distribution in LPB-treated Ti-6Al-4V [30]. Thus, one may conclude that a parabolic relationship can be established

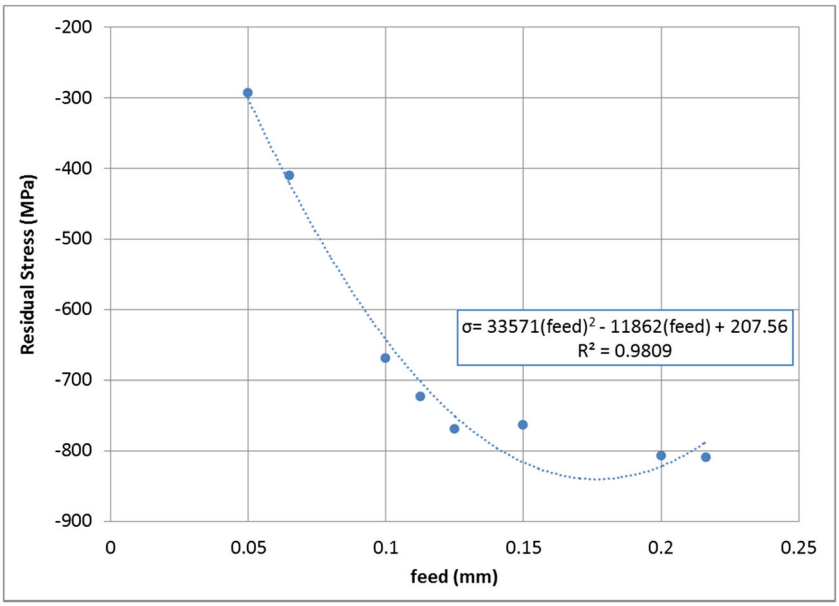

Fig. 11 Effect of the feed on tangential residual stress on the surface (σ_0)

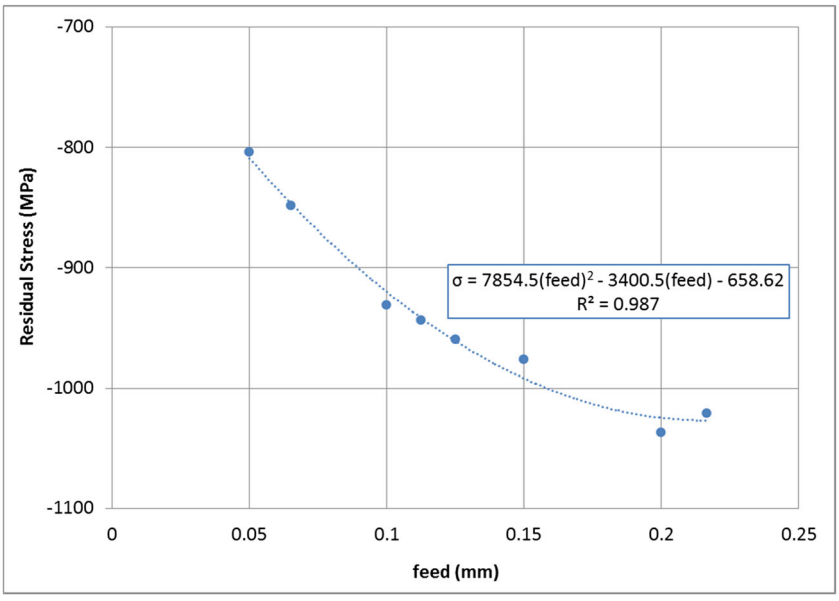

Fig. 12 Effect of the feed on the tangential residual stress at Z_{min} (σ_{min})

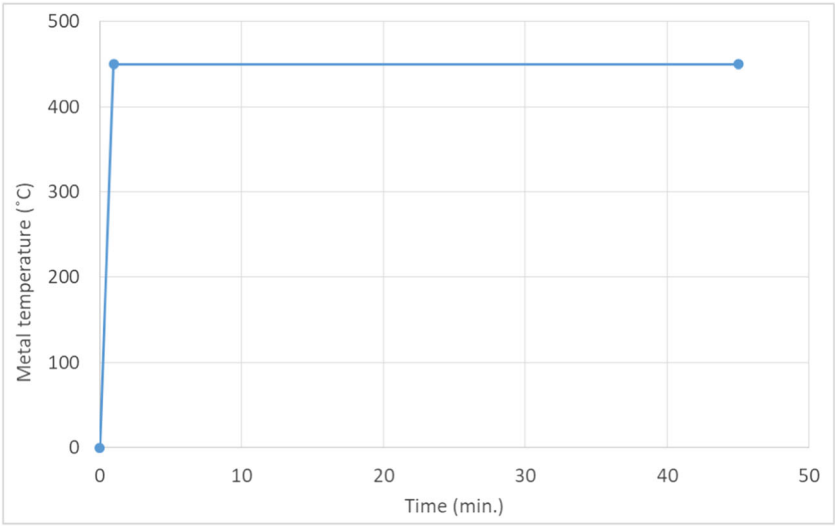

Fig. 13 Time plot of metal temperature to be used in thermal relaxation simulation

between the residual stresses with respect to the feed. Therefore, the developed FE model can describe the variation of the process parameters on the residual stress profile.

6 FE model of thermal relaxation

The residual stress and strain states at the end of spring-back simulation are provided as initial condition for the subsequent thermal relaxation analysis conducted in ABAQUS/Standard.

The FE analysis for thermal relaxation is a steady-state thermomechanical analysis followed by a viscoplastic analysis to account for creep relaxation in the surface layer. An arbitrary time step was assigned to steady-state analysis (here 10 s) since the time has no role in the FE analysis at this stage. However, the step time is important for the creep analysis and it is assumed to be the same as the annealing process (45 min at 450 °C) considered in experimental study of Nalla et al. [26]. The thermal loading is applied as the bulk metal temperature increases to 450 °C and then dwelling for 45 min as illustrated in Fig. 13.

ABBAQUS/Standard employs a backward-difference scheme in the thermal-stress analysis to integrate temperatures, and the non-linear coupled system of stress (displacement) and temperatures are solved using Newton's method.

As explained earlier, the JC model was used in the simulation of DCR process which involves a high strain rate deformation. The JC model parameters are obtained by fitting the model coefficients to plastic deformations under high strain rate regimes while the spring back and thermal relaxation processes occurs under a quasi-static or steady-state condition. Therefore, JC model, especially with original parameter values, might not be a good representative of the plastic deformation of the material during thermal relaxation.

In an attempt to overcome this problem, Zhou et al. [42] recalibrated parameter m (which describes the thermal softening of yield stress) of their assumed JC model to analyze thermal relaxation of residual stress induced in laser-shot-peened Ti-6Al-4V plate. However, this still is not representing the quasi-static nature of the thermal relaxation stage since the other JC parameters (i.e. A, B, and n) had been extracted from high strain rate test data.

In the present study, temperature-dependent quasi-static stress-strain curves in form of isotropic plasticity based on true stress and strain measurements by Haight et al. [11] are utilized in the developed FE model. The true stress-strain data at strain rate of 1 s^{-1} for Ti-6Al-4V alloy at different temperatures are shown in Fig. 14. The thermal relaxation stage is then performed using a viscoplastic model which couples the creep

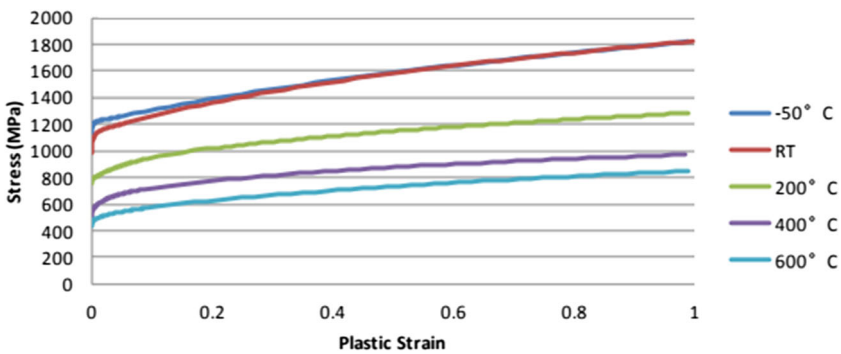

Fig. 14 Temperature-dependent plastic deformation of Ti-6Al-4V at strain rate 1 s^{-1} [11]

Table 3 Hyperbolic creep coefficients for 450 °C

A (s^{-1})	6.33034E−15
B (MPa)	0.0435
n	1.000504
H (kJ/(mol·K))	200

and plasticity deformation mechanisms to predict the state of residual stresses at the elevated temperature.

Norton and hyperbolic-sine function are widely used creep laws and have been employed to describe the creep behavior of Ti-6Al-4V [34, 35]. Hyperbolic-sine creep model which has been found to be suitable for the primary creep can be described as

$$\dot{\varepsilon}_c = A(sinhB\sigma)^n \exp\left(-\frac{\Delta H}{RT}\right) \tag{12}$$

where T is temperature [K], ΔH is creep activation energy [kJ/(mol·K)], R is gas constant [kJ/mol], A is material structure factor [s^{-1}], B is stress level factor [MPa^{-1}], n is stress exponent.

All the available creep models in the literatures have been developed either for long time deformations where the data have been fit to the secondary creep [12, 34] or at the temperatures above 450 °C [14]. The only short-term creep strains and stresses available in the open-source literatures were found in [5, 12] where the minimum reported dwell time is 1 h.

Prevey et al. [29] claimed that the thermal relaxation of residual stress induced by shot peening, gravity peening, and laser shocking in Ti-6Al-4V and Inconel 718 materials shows strong correlation with the amount of induced cold work and the initial relaxation of compression residual stress appears to be time independent in both material. Therefore, it was assumed that the creep relaxation developed based on test data at 1 h dwelling time is also applicable for 45 min. A new set of hyperbolic creep law coefficients are constructed in the current study that has the best fit to those experimental measurement data points available in [5, 12], in order to describe the primary creep at 450 °C and are presented in Table 3.

6.1 Validation of the FE model for thermal relaxation

The profile of residual stress in tangential direction, σ_{zz}, at elevated temperature was obtained using the developed FE model along the same lines where the stresses were acquired at room temperature. The results are shown in Fig. 15 and compared to experimental measurements of Nalla et al. [26].

Zener-Wert-Avramin model is an analytical function which describes the thermal relaxation of macro-residual stresses and changes of work hardening states quantitatively and it is applicable to a wide range of temperatures. The function formulates the thermal relaxation based on activation enthalpy which is roughly the enthalpy for self-diffusion. Zener-Wert-Avramin model to describe the residual stress relaxation during thermal loading can be written as [33, 41, 42]

$$\frac{\sigma^{rs}(T,t)}{\sigma_0^{rs}} = exp\left\{-\left[Cexp\left(\frac{-\Delta H_A}{\kappa T}\right)t\right]^m\right\} \tag{13}$$

where $\sigma^{rs}(T,t)$ is the residual stress value after annealing at temperature T and time t. σ_0^{rs} is the initial residual stress. ΔH_A is the activation enthalpy and C is velocity constant. κ is Boltman constant and m represents material property parameter found by the experimental test. Stanojevic et al. [34] determined the parameters of this model for axial and tangential stress relaxation in deep-rolled Ti-6Al-4V as provided in Table 4.

Zener-Wert-Avramin model has also been utilized in the present work to predict the profile of tangential residual stress

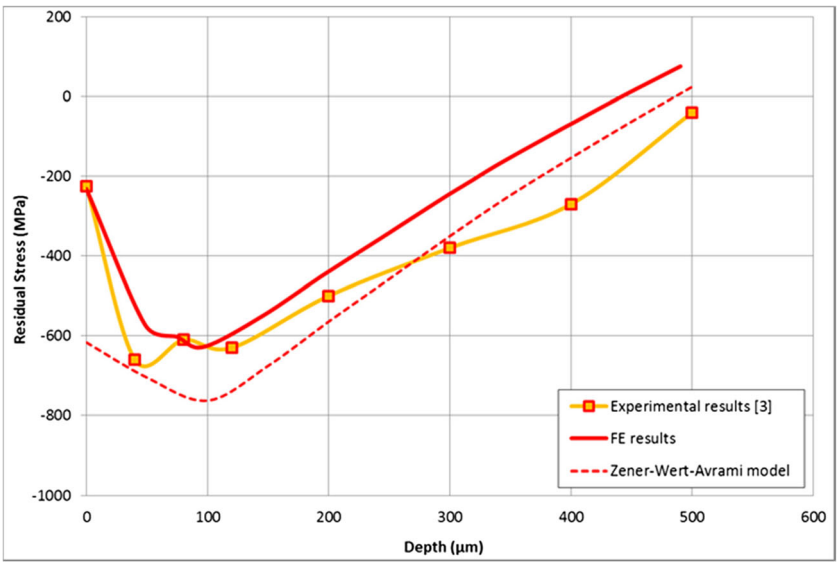

Fig. 15 Residual stress profiles in tangential direction at 450 °C

Table 4 Zener-Wert-Avrami parameters in axial and tangential direction of deep-rolled Ti-6Al-4V [34]

Parameter	Axial	Tangential
C *[1/s]*	3.96 E5	8.11 E4
ΔH_A *[eV]*	1.176	1.098
m *[−]*	0.2061	0.3132

after thermal relaxation for the sake of comparison with the experimental measurements and FE results as shown in Fig. 15. The results show the superiority of the developed FE to the analytical Zener-Wert-Avramin model as it agrees better with the experimental measurements.

The noticeable deviation between FE and experimental results in region above 200 μm depth in Fig. 15 is mainly associated with the fact that the experimental measured residual stress has not been corrected to account for the effect of surface layer removals, standard deviation difference in creep behavior of Ti-64 provided by different suppliers and also assumptions related to the material model. Results in Fig. 15 also demonstrate that although the analytical model can predict the residual stress in a depth above 200 μm rather well, it fails to predict the magnitude of the residual stress on the surface layer and near subsurface layers. This may be attributed to the fact that the analytical model assumes constant activation energy and parameter *C* through the thickness. It is also noted that empirical models need to be recalibrated for each surface treatment process and associated control parameters. Moreover, these models do not generally incorporate material microstructure, hardening behavior, plastic strain, and the underlying physical deformation mechanisms which have a significant role in the stress relaxation.

6.2 Effect of elevated temperature on the induced residual stress distribution

The distribution of residual stress in axial (σ_{xx}) and tangential (σ_{zz}) directions at room and elevated temperature 450 °C are shown in Fig. 16 for the sake of comparison. The results clearly confirm that the thermal relaxation redistributes the residual stresses which leads to a more uniform stress profiles through the depth and reduces the anisotropy of the residual stresses as the difference between σ_{xx} and σ_{zz} reduces at the elevated temperature.

As it can be realized, the induced residual stresses in DCR process substantially relaxes at the elevated temperature. This should be carefully taken into consideration as improper selection of process parameters may induce beneficial residual stresses which may be completely released at the elevated temperature and thus drastically reducing the fatigue life enhancement of the components. This suggests that any future design optimization on the selection of the optimal process parameters should be conducted at the operating temperature.

7 Conclusion

A high-fidelity finite element (FE) model has been developed to predict the distribution of the residual stresses induced by the DCR process on Ti-6Al-4V material at room temperature and the subsequent thermal relaxation at elevated temperature. The results obtained from the developed FE model correlates well with the available experimental measurements. The FE model can accurately capture both the shape and magnitude of the residual stress profiles up to depth of 200 μm from the surface. In deeper depth, the numerical and experimental

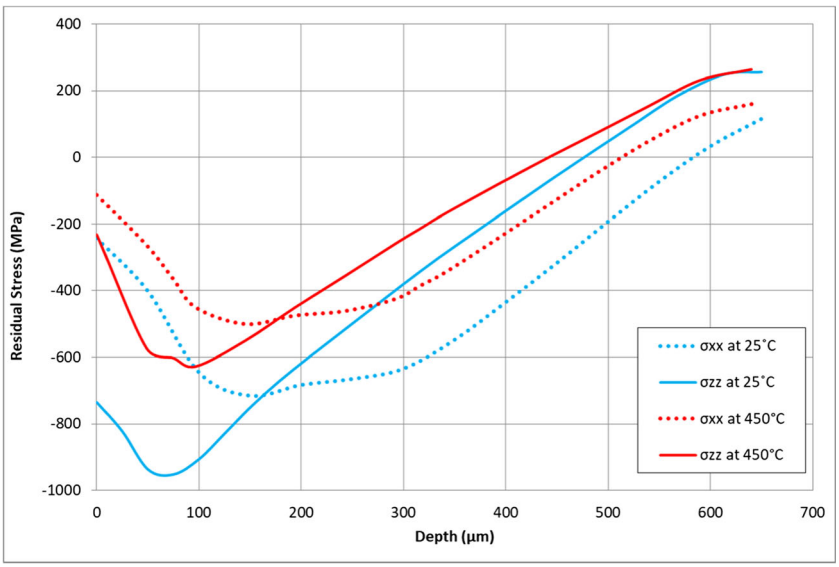

Fig. 16 Residual stress profile in axial and tangential direction at 450 °C

results deviate slightly mainly due to the layer removal involved in the experimental measurement.

It was discussed that deep rolling process changes the microstructure of the specimen in the surface layer which leads to changes in mechanical behavior of the material. In the current work, a proper deformation mechanism was adopted based on dominating deformation mechanism associated to the microstructure of the treated materials. At the surface layer where the dislocation density is high, the deformation is controlled by dislocation glide which results in primary creep deformation. However, in deeper depths, the main controlling relaxation mechanism is plastic deformation due to softening of the material at higher temperature. A hyperbolic-sine creep law used for primary creep deformation of Ti-6Al-4V at 450 °C has been employed for thermal relaxation stage of the modeling. The conclusions and highlights of the present study are summarized as follows:

1. A minimum number of rolling passes is required to reach the steady state of the residual stress field. The residual stress profile needs to be obtained in the steady-state region whereby further rolling the workpiece; the residual stress state does not change.
2. The CDR process introduces an anisotropic residual stress in the material. The residual stress in the rolling direction (axial) is considerably lower than the stress component perpendicular to the rolling direction (tangential).
3. Increasing the feed raises the minimum and surface-compressive residual stresses when the other process parameters (ball diameter and pressure) are kept unchanged.
4. The developed FE model is able to predict the thermal relaxation of the residual stresses at the region of interest near the surface with a reasonable accuracy while Zener-Wert-Avrami analytical model fails to capture the magnitude and profile of the relaxed residual stresses.
5. Thermal relaxation redistributes the residual stresses which lead to a more uniform stress profile through the depth with less anisotropy of the residual stresses.

References

1. Altenberger I (2003) Alternative mechanical surface treatments: microstructures, residual stresses & fatigue behavior. In: Lothar Wagner (ed) Shot Peening. Wiley-VCH Verlag GmbH & Co., KGaA, Weinheim, FRG, p 419–434
2. Altenberger I (2005) Deep rolling—the past, the present and the future. In: proceedings of 9th international conference on shot peening, sept 6–9 (Paris, France), p 144
3. Altenberger I, Nalla R, Noster U et al (2002) On the fatigue behavior and associated effect of residual stresses in deep-rolled and laser shock peened Ti-6Al-4V alloys at ambient and elevated temperatures. University of California, Berkeley, p 94720
4. Bäcker V, Klocke F, Wegner H, Timmer A, Grzhibovskis R, Rjasanow S (2010) Analysis of the deep rolling process on turbine blades using the FEM/BEM-coupling. IOP Conference Series: Materials Science and Engineering 10(1):012134
5. Badea L, Surand M, Ruau J et al (2014) Creep behavior of Ti-6Al-4V from 450° C to 600° C. U.P.B.Sci.Bull. Series B 76(1):185–196
6. Balland P, Tabourot L, Degre F, Moreau V (2013) Mechanics of the burnishing process. Precis Eng 37(1):129–134
7. Balland P, Tabourot L, Degre F, Moreau V (2013) An investigation of the mechanics of roller burnishing through finite element simulation and experiments. Int J Mach Tools Manuf 65:29–36
8. Buchanan DJ, John R, Brockman RA, Rosenberger AH (2010) A coupled creep plasticity model for residual stress relaxation of a shot-peened nickel-based superalloy. JOM J Miner Met Mater Soc 62(1):75–79
9. Cook RD (2007) Concepts and applications of finite element analysis. John Wiley & Sons, New York
10. Gill C, Fox N, Withers P (2008) Shakedown of deep cold rolling residual stresses in titanium alloys. J Phys D 41(17):174005
11. Haight S, Wang L, Du Bois P et al (2016) Development of a titanium alloy Ti-6Al-4V material model used in LS-DYNA DOT/FAA/TC-15/23
12. Jenkins JM (1984) Effect of creep in titanium alloy Ti-6Al-4V at elevated temperature on aircraft design and flight test NASA-TM-86033, H-1228, NAS 1.15:86033
13. Jiang Y, Xu B, Sehitoglu H (2002) Three-dimensional elastic-plastic stress analysis of rolling contact. J Tribol 124(4):699–708
14. Junjie X, Dongsheng L, Xiaoqiang L (2015) Modeling and simulation for the stress relaxation behavior of Ti-6Al-4V at medium temperature. Rare Metal Mater Eng 44(5):1046–1051
15. Kıranlı E (2009) Determination of material constitutive equation of a biomedical grade Ti6AI4V alloy for cross-wedge rolling. Master of Science in Material Science, Izmir institute of technology
16. Klocke F, Bäcker V, Wegner H, Timmer A (2009) Innovative FE-analysis of the roller burnishing process for different geometries. In: X international conference on computational plasticity fundamentals and applications, Barcelona, Spain.
17. Klocke F, Bäcker V, Wegner H, Zimmermann M (2011) Finite element analysis of the roller burnishing process for fatigue resistance increase of engine component. Proc Inst Mech Eng B J Eng Manuf 225(1):2–11
18. Lee W, Lin C (1998) Plastic deformation and fracture behaviour of Ti–6Al–4V alloy loaded with high strain rate under various temperatures. Mater Sci Eng A 241(1):48–59
19. Lesuer DR (2000) Experimental investigation of material models for Ti-6Al-4V and 2024-T3. FAA report DOT/FAA/AR-00/25
20. Li F, Xia W, Zhou Z (2010) Finite element calculation of residual stress and cold-work hardening induced in Inconel 718 by low plasticity burnishing. In: 2010 Third International Conference on Information and Computing, 2 vol. IEEE, p 175
21. Lim A, Castagne S, Wong CC (2016) Effect of deep cold rolling on residual stress distributions between the treated and untreated regions on Ti–6Al–4V alloy. J Manuf Sci Eng 138(11):111005
22. Liu Y, Wang L, Wang D (2011) Finite element modeling of ultrasonic surface rolling process. J Mater Process Technol 211(12):2106–2113
23. Loh N, Tam S, Miyazawa S (1989) Statistical analyses of the effects of ball burnishing parameters on surface hardness. Wear 129(2):235–243
24. Majzoobi G, Jouneghani FZ, Khademi E (2016) Experimental and numerical studies on the effect of deep rolling on bending fretting fatigue resistance of Al7075. Int J Adv Manuf Technol 82(9–12):2137–2148

25. Mohammadi F, Sedaghati R, Bonakdar A (2013) Finite element analysis and design optimization of low plasticity burnishing process. Int J Adv Manuf Technol 70(5–8):1337–1354
26. Nalla RK, Altenberger I, Noster U, Liu GY, Scholtes B, Ritchie RO (2003) On the influence of mechanical surface treatments-deep rolling and laser shock peening-on the fatigue behavior of Ti-6Al-4V at ambient and elevated temperatures. Mater Sci Eng A 355(1–2):216–230
27. Nikitin I, Altenberger I, Maier H et al (2005) Mechanical and thermal stability of mechanically induced near-surface nanostructures. Mater Sci Eng A 403(1):318–327
28. Nițu E, Iordache M, Marincei L, Charpentier I, le Coz G, Ferron G, Ungureanu I (2011) FE-modeling of cold rolling by in-feed method of circular grooves. J Mech Eng 57(9):667–673
29. Prevéy P, Hombach D, Mason P (1998) Thermal residual stress relaxation and distortion in surface enhanced gas turbine engine components. In: Milam DL (ed) Proceedings of the 17th heat treating society conference. ASM, Indianapolis Sept 15–18, 1997
30. Prevéy PS, Shepard MJ, Smith PR (2001) The effect of low plasticity burnishing (LPB) on the HCF performance and FOD resistance of Ti-6AI-4V. In: the 6th National Turbine Engine High Cycle Fatigue (HCF) Conference, 5–8 March 2001. Jacksonville, Florida, USA. DTIC Document
31. Sartkulvanich P, Altan T, Jasso F, Rodriguez C (2007) Finite element modeling of hard roller burnishing: an analysis on the effects of process parameters upon surface finish and residual stresses. J Manuf Sci Eng 129(4):705–716
32. Sayahi M, Sghaier S, Belhadjsalah H (2013) Finite element analysis of ball burnishing process: comparisons between numerical results and experiments. Int J Adv Manuf Technol 67(5–8):1665–1673
33. Schulze V (2006) Modern mechanical surface treatment: states, stability, effects. Wiley-VCH, New York
34. Stanojevic A, Angerer P, Oberwinkler B (2016) Thermal stability of residual stresses in Ti-6Al-4V components. IOP Conference Series: Materials Science and Engineering 119(1):012007
35. Stanojevic A, Maderbacher H, Angerer P et al (2016) Stability of residual stresses in Ti-6Al-4V components due to mechanical loads. In: Venkatesh V (ed) Proceedings of the 13th world conference on titanium. Wiley Online Library, Hoboken, p 1593
36. Sun J, Guo Y (2009) Material flow stress and failure in multiscale machining titanium alloy Ti-6Al-4V. Int J Adv Manuf Technol 41(7):651–659
37. Dassault Systèmes (2013) Volume II: analysis. In: ABAQUS 6.13, Analysis User's guide
38. Trauth D, Klocke F, Mattfeld P, Klink A (2013) Time-efficient prediction of the surface layer state after deep rolling using similarity mechanics approach. Proc CIRP 9:29–34
39. Tsuji N, Tanaka S, Takasugi T (2008) Evaluation of surface-modified Ti–6Al–4V alloy by combination of plasma-carburizing and deep-rolling. Mater Sci Eng A 488(1):139–145
40. Yen Y, Sartkulvanich P, Altan T (2005) Finite element modeling of roller burnishing process. CIRP Ann Manuf Technol 54(1):237–240
41. Zaroog OS, Ali A, Zahari B et al (2009) Modelling of residual stress relaxation: a review. Pertanika J Sci Technol 17(2):211–218
42. Zhou Z, Bhamare S, Ramakrishnan G, Mannava SR, Langer K, Wen Y, Qian D, Vasudevan VK (2012) Thermal relaxation of residual stress in laser shock peened Ti–6Al–4V alloy. Surf Coat Technol 206(22):4619–4627
43. Zhuang W, Wicks B (2004) Multipass low-plasticity burnishing induced residual stresses: three-dimensional elastic-plastic finite element modelling. Proc Inst Mech Eng C 218(6):663–668